Time behavior of the secondary flow between time-periodically corotating cylinders: A two-frequency forcing case

P. Ern[1] and J.-E. Wesfreid[2]
[1]*Institut de Mécanique des Fluides, UMR CNRS/UPS-INP 5502, Allée du Professeur Camille Soula, 31400 Toulouse, France*
[2]*Laboratoire de Physique et Mécanique des Milieux Hétérogènes, UMR CNRS 7636, Ecole Supérieure de Physique et Chimie Industrielles (ESPCI), 10 rue Vauquelin, 75231 Paris cedex 05, France*
(Received 16 August 2001; published 15 March 2002)

We consider the oscillatory flow between time-periodically corotating cylinders, in the case of a two-frequency forcing. The angular velocity $\Omega(t)$ of the cylinders is the sum of a low-frequency ω_1 oscillation plus a harmonic frequency ω_2 oscillation at a lower amplitude, $\Omega(t)=\Omega_1\cos(\omega_1 t)+\Omega_2\cos(\omega_2 t)$. The temporal behavior of the secondary flow is characterized by ultrasound Doppler velocimetry. For a single-frequency forcing at ω_1, above a critical amplitude Ω_1, within one cycle, the secondary flow measurements exhibit a spikelike behavior with several successive growths, dampings, and periods of quietness. The effect of the superimposed ω_2 frequency is the following, although if alone it would be stable: to sharpen the spikes, restabilizing the flow for some intervals that exhibit secondary flow for the single forcing at ω_1; and to induce further secondary flow spikes during what is a quiescent stage in the single ω_1 frequency forcing case. Numerical calculations for the finite-gap quasisteady linear stability analysis are presented and provide a good prediction of the times of growth and damping of the secondary flow observed experimentally during a flow period.

DOI: 10.1103/PhysRevE.65.047301 PACS number(s): 47.20.Cq, 47.54.+r, 47.62.+q

Recently, the effect of a spatially periodic or time-periodic perturbation on a primary bifurcation has been studied for hydrodynamical flows both theoretically and experimentally [1,2]. In particular, the influence of a temporal modulation on a spatiotemporal pattern has been studied in the cases of surface waves patterns excited by two-frequency forcing [3] and of time-periodic thermal convection forced with an external frequency [4,5]. In contrast with these works, we here consider the stability of a base flow generated by a two-frequency external forcing. We use a Taylor-Couette geometry where the fluid is confined between two *jointly* corotating cylinders. The rotation is the sum of a low-frequency oscillation plus a higher-frequency harmonic oscillation at a lower amplitude. Several open questions arise in this situation concerning the instability onset, the frequency interaction, and the time dependence of secondary flow. We focus our attention on the last two points. In particular, the effect of the additional modulation is underlined by comparison with the single-frequency forcing case. In previous works [6,7], we studied the flow between time-periodically corotating cylinders, the angular velocity Ω of both cylinders having a mean value Ω_m and modulation amplitude Ω_0 as $\Omega(t)=\Omega_m+\Omega_0\cos(\omega t)$. We established a finite-gap analytical expression for the purely azimuthal basic flow. The flow instability, with a threshold characterized by the Taylor number T_a, was studied as a function of the rotation number N_R, the frequency γ, and the gap size δ, defined by

$$T_a=\frac{\Omega_0 R^{1/2} d^{3/2}}{\nu},\quad N_R=\frac{\Omega_m}{\Omega_0}\frac{d}{R},\quad \gamma=\left(\frac{\omega d^2}{2\nu}\right)^{1/2},$$

$$\text{and}\quad \delta=\frac{d}{R},$$

ν being the viscosity, d the gap width, and R the inner cylinder radius. Secondary flow corresponds to counterrotating vortices evolving in time. The temporal behavior of secondary flow was studied experimentally for different values of the parameters. In particular, we showed that secondary flow grows and damps several times during a flow cycle. Numerical and analytical results obtained with a quasisteady finite-gap linear stability analysis were shown to be in good agreement with the experimental secondary flow behavior for $\gamma\leqslant 1$.

We are here interested in the time dependence of the secondary flow in the case of a two-frequency forcing, the angular rotation of both cylinders being

$$\Omega(t)=\Omega_1\cos(\omega_1 t)+\Omega_2\cos(\omega_2 t).$$

We denote by τ_1 and τ_2 the periods of the frequencies ω_1 and ω_2.

The experimental setup, the measuring technique, and the operating procedure are the same as those described by [7]. Instantaneous velocity profile measurements are obtained with an ultrasound Doppler velocimeter (Signal Processing Dop 1000) in the rotating frame of the cylinders. The real time evolution of $w(z,t)$ the axial velocity profile along the axial direction z shows a repeated growth and decay in the amplitude of axial flow. At any time t, we characterize the secondary flow by the root-mean-square value

$$W_{\mathrm{rms}}(t)=\left(\frac{1}{N}\sum_{i=1}^{N} w^2(z_i,t)\right)^{1/2}.$$

We illustrate here the particular parameter values

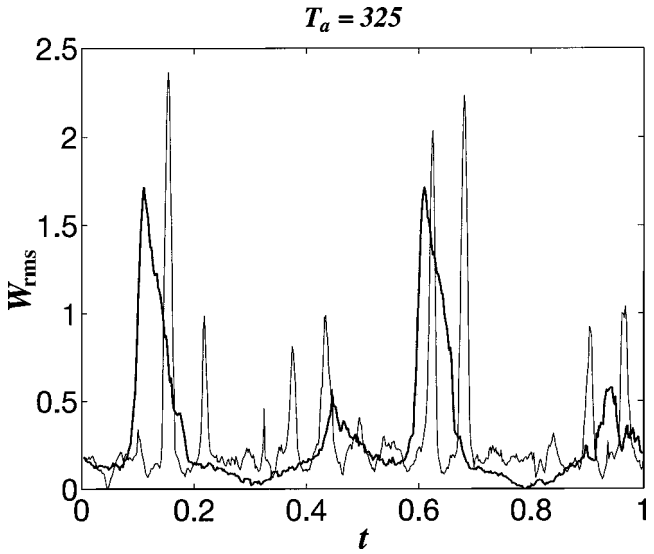

FIG. 1. Experimental behavior of $W_{\mathrm{rms}}(t)$ (in mm/s) over one flow period for $T_a=325$ ($\delta=0.112$) in the case of a two-frequency forcing at $\gamma(\omega_1)=1$ with $\gamma(\omega_2)=4$ (thin curve) and of a single-frequency forcing at $\gamma=1$ (thick curve).

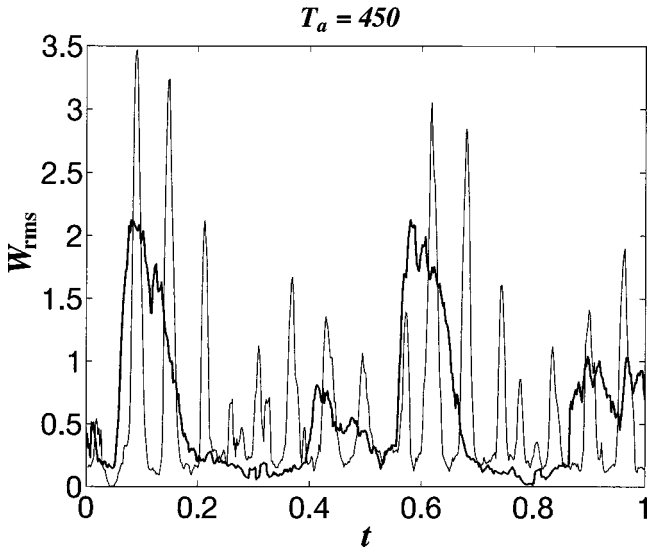

FIG. 2. Experimental behavior of $W_{\mathrm{rms}}(t)$ (in mm/s) over one flow period for $T_a=450$ ($\delta=0.112$) in the case of a two-frequency forcing at $\gamma(\omega_1)=1$ with $\gamma(\omega_2)=4$ (thin curve) and of a single-frequency forcing at $\gamma=1$ (thick curve).

$$\gamma(\omega_1)=1, \quad \gamma(\omega_2)=4, \quad \frac{\Omega_2}{\Omega_1}=0.2, \quad \delta=0.112 \quad \text{with}$$

$$T_a=\frac{\Omega_1 R^{1/2} d^{3/2}}{\nu}.$$

This situation corresponds to a frequency ratio $\omega_2/\omega_1=16$. The basic flow is given as $V_{B,2F}(x,t)=V_{B,\mathrm{LF}}(x,t)+V_{B,\mathrm{HF}}(x,t)$, by the superposition of the basic flows $V_{B,\mathrm{LF}}(x,t)$ for $\gamma=1$ and $V_{B,\mathrm{HF}}(x,t)$ for $\gamma=4$ with amplitude Ω_2/Ω_1, expressions for these being given in [6,7]. Note that the instability threshold for a single-frequency forcing at $\gamma=1$ is close to the instability threshold for a single-frequency forcing at $\gamma=4$ (roughly $T_a\simeq 200$, see [8]) and that as a consequence of the ratio chosen for the amplitudes of the two modulations, for the Taylor numbers considered ($T_a \leqslant 500$), the modulation for $\gamma=4$, if considered alone, would be stable.

Figure 1 shows for $T_a=325$ the evolution of $W_{\mathrm{rms}}(t)$ over one cycle for the two-frequency forcing at $\gamma(\omega_1)=1$ and $\gamma(\omega_2)=4$ (thin curve) and for a single-frequency forcing at $\gamma=1$ (thick curve). The Taylor number T_a is calculated using the amplitude Ω_1, with an error lower than 3.5% due to the viscosity estimation. The period is one cycle for $\gamma=1$ (roughly 86 s) and is scanned with about 518 data points. The time origin of data acquisition has been chosen to be the moment when the rotation of the cylinders changes sign. The peaks correspond to successive growth and damping of secondary flow (four times for $\gamma=1$). For a destabilizing forcing at the single frequency $\gamma=4$, the evolution of $W_{\mathrm{rms}}(t)$ during a cycle, not reproduced here, shows two large peaks of secondary flow. The comparison between the two plots of Fig. 1 shows that secondary flow peaks are strongly reduced in width in the two-frequency forcing case. Maximum peak width is about half a period of the higher-frequency modulation, roughly 2.5 s. In particular, around the times $t\approx 0.1$ and $t\approx 0.6$, the high-amplitude peaks for $\gamma=1$ are split in thin peaks. This windowing on the secondary flow temporal regions induced by the higher frequency becomes even more evident for higher Taylor number T_a, as exemplified in Fig. 2 for $T_a=450$.

For a single-frequency forcing at $\gamma \leqslant 1$, Ern and Wesfreid [7] showed that a prediction of the secondary flow temporal

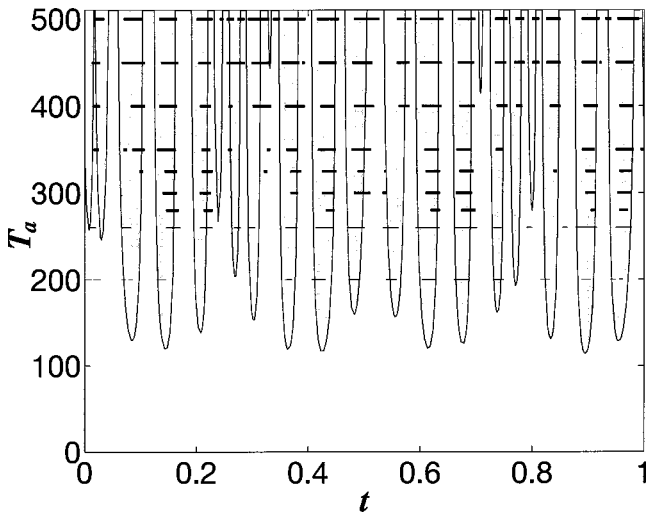

FIG. 3. Instantaneous critical Taylor numbers for the two-frequency forcing at $\gamma(\omega_1)=1$ with $\gamma(\omega_2)=4$ obtained numerically over one flow cycle with a finite-gap quasisteady linear stability analysis ($\delta=0.112$). Regions inside the curves indicate quasisteady unstable flow conditions. The horizontal lines for different T_a values correspond to the $W_{\mathrm{rms}}(t)$ peak widths observed experimentally for an amplitude of $W_{\mathrm{rms}}=0.15$ (thin lines) and $W_{\mathrm{rms}}=0.3$ mm/s (thick lines).

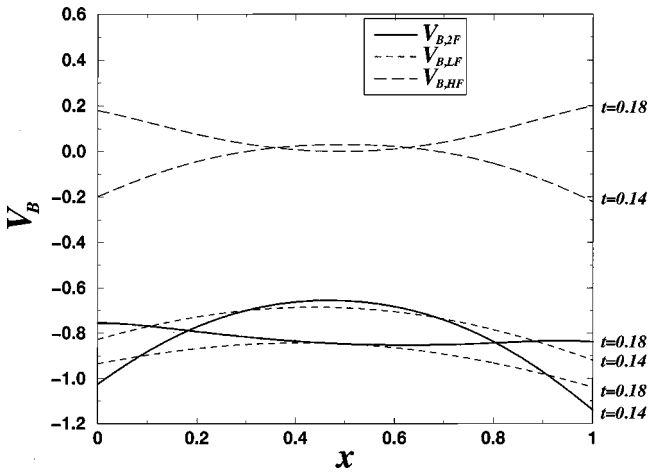

FIG. 4. Profile across the gap x for the times $t=0.14$ and $t=0.18$ of the base flow velocities for a single-frequency forcing $V_{B,\mathrm{LF}}$ at $\gamma=1$ and $V_{B,\mathrm{HF}}$ at $\gamma=4$, and for a two-frequency forcing $V_{B,2F}=V_{B,\mathrm{LF}}+V_{B,\mathrm{HF}}$ at $\gamma=1$ with $\gamma=4$.

regions is given over a flow period by the quasisteady finite-gap linear stability analysis. We use the same numerical procedure for the case of the two-frequency forcing. Neutral and axisymmetric perturbations are considered. Figure 3 shows the instantaneous critical Taylor numbers obtained at any fixed time t_0 over a period for the corresponding basic flow $V_{B,2F}(x,t_0)$. Regions inside the curves correspond to unstable flow conditions. Comparison with Figs. 1 and 2 shows that there is a good agreement between experiments and numerical calculations. To facilitate the comparison for different Taylor numbers T_a, we have reported on the numerical results of Fig. 3 the temporal widths of the experimental peaks for the amplitude $W_{\mathrm{rms}}=0.15$ mm/s for $T_a=200$ and 260 (thin lines) and $W_{\mathrm{rms}}=0.3$ mm/s for $T_a=280$, 300, 325, 350, 400, 450, and 500 (thick lines), obtained by [9]. These amplitudes were chosen as a compromise between discriminating the maximum number of peaks and measuring their maximal width. In particular, the windowing at τ_2 of the higher frequency over the secondary flow temporal regions of $\gamma=1$ is well-recovered numerically. This peak windowing can be explained in the quasisteady calculations by considering the evolution in time of the basic flow profile in the gap, as illustrated in Fig. 4 for the times $t=0.14$ and 0.18. For $t\approx0.14$, both $V_{B,\mathrm{HF}}$ and $V_{B,\mathrm{LF}}$ are negative, the resulting basic flow has an accentuated curvature and the flow is found to be unstable. For $t\approx0.18$ on the contrary, the $V_{B,\mathrm{HF}}$ and $V_{B,\mathrm{LF}}$ curvatures compensate. The resulting $V_{B,2F}$ is then nearly uniform over the gap, giving quasisteady stability. This is in keeping with Rayleigh's [10] and Hall's [11] stability criterion in its finite-gap formulation, the minimum value over the gap width of the instantaneous finite-gap Rayleigh discriminant being negative for $t\approx0.14$ and positive for $t\approx0.18$. Also interesting is the numerical prediction around the times $t\approx0.3$ and 0.8. Around these times, the flow is stable at the single frequency $\gamma=1$. Here, in the presence of $\gamma=4$, we see the existence of a temporal unstable region each half a period $\tau_2/2$ of the $\gamma=4$ modulation. Experimentally, this behavior is more clearly observed around the time $t\approx0.8$ in Fig. 2, where secondary flow peaks appear every $\tau_2/2$.

These results show good agreement for the time-dependent behavior of secondary flow between the experiments and a finite-gap stability analysis assuming both quasisteadiness and linearity. Most notable is the agreement with the prediction of the finite-gap quasisteady calculations that the secondary flow experiences over one cycle of about 20 successive growth and damping events, with a well-defined periodicity (either τ_2 or $\tau_2/2$). The particular times of appearance and disappearance of secondary flow are also provided, generally with a slight anticipation. The fact that the linear analysis is in good agreement with experimental results suggest the following interpretation of the secondary flow behavior. Two types of secondary flow are observed. The first, near the times $t\approx0.1$, 0.4, 0.6, and 0.9, corresponds to $\gamma=1$ secondary flow modified by the presence of the higher frequency $\gamma=4$, the main effect of this modulation being the peak windowing. A physical explanation of flow restabilization leading to this peak windowing could account on the fact that, for a forcing at a single frequency, the vortex structure reverses its rotation half a period later [7]. We suggest that the peaks appear when the vortex structures induced by both frequencies rotate in the same direction. Half a $\gamma=4$ period later, the tendency of the $\gamma=4$ structures to revert their rotation direction may damp the vortex structure. This seems also supported by the fact that the two-frequency peaks for instance around $t\approx0.1$ and $t\approx0.6$ are not located in the same place with respect to the $\gamma=1$ peaks but are shifted by $\tau_2/2$. The second type of secondary flow is the one around $t\approx0.3$ and 0.8, when $\gamma=1$ alone would have been stable, and is due to the higher frequency $\gamma=4$ oscillation superimposed to the basic flow of $\gamma=1$, which is at that time close to a uniform rotation around its maximum amplitude. This flow is known to be unstable each $\tau_2/2$ [7].

Further work includes variation of parameters such as the frequency ratio $R_\gamma=\gamma(\omega_2)/\gamma(\omega_1)$ and the amplitude ratio $R_\Omega=\Omega_2/\Omega_1$. In particular, in the range of validity for R_γ and R_Ω of a linear analysis, the numerical prediction of the secondary flow temporal behavior may be extended to more general periodic forcings. The effect of these parameters on the instability threshold also deserves investigation.

[1] P. Coullet and D. Walgraef, Europhys. Lett. **10**, 525 (1989).
[2] H. Kuhlmann, D. Roth, and M. Lücke, Phys. Rev. A **39**, 745 (1989).
[3] M. Silber and A. Skeldon, Phys. Rev. E **59**, 5446 (1999).
[4] A. Chiffaudel and S. Fauve, Phys. Rev. A **35**, 4004 (1987).
[5] H. Riecke, J. Crawford, and E. Knobloch, Phys. Rev. Lett. **61**, 1942 (1988).
[6] P. Ern, C. R. Acad. Sci., Ser. IIb: Mec., Phys., Chim., Astron.

326, 727 (1998).
[7] P. Ern and J.-E. Wesfreid, J. Fluid Mech. **397**, 73 (1999).
[8] A. Aouidef, C. Normand, A. Stegner, and J.-E. Wesfreid, Phys. Fluids **6**, 3665 (1994).
[9] P. Ern, Thèse de Doctorat, Université Paris VI, 1997.
[10] Lord Rayleigh, Proc. R. Soc. London, Ser. A **93**, 148 (1916).
[11] P. Hall, J. Fluid Mech. **124**, 475 (1982).